actuators

MDPI

Article

Isometric Force Characterization of Braided Pneumatic Actuators

Ben Bolen, Mohammad Elzein, Lawrence Pang and Alexander Hunt *

Department of Mechanical and Materials Engineering, Portland State University, Portland, OR 97207, USA; bbolen83@gmail.com (B.B.); melzein@pdx.edu (M.E.)
* Correspondence: ajh26@pdx.edu

Highlights

- Braided Pneumatic Actuator maximum isometric force is a function of resting length.
- Force curves are normalized with pressure and maximum contraction.
- A high-fidelity predictive force model is developed using few coefficients.

Abstract

Artificial muscles such as braided pneumatic actuators (BPAs) offer many advantages for robotic systems, including high durability and strength-to-weight ratios. However, their use in robotic systems is still extremely limited, in part due to their poor force, length, and pressure characterization. In this work, a test setup is created to compare force produced by Festo fluidic BPAs with leading models. Our analysis of the data has resulted in (1) the development of new equations to calculate force as functions of pressure and contraction for Festo BPAs with uninflated diameters of 10 mm and 20 mm, and (2) a novel equation for the maximum force in 10 mm and 20 mm diameter Festo BPAs as a function of their resting length. This will lead to faster design processes and the development of new systems such as biomimetic robots that are able to more accurately reproduce the range of motion and isometric torque profiles that exist in the animals they are mimicking.

Keywords: BPA; biomimetic; function fit; PAM; artificial muscle; isometric force

1. Introduction

Biomimetic robots provide a platform for investigating how mechanical structure and control interact to generate movement, offering complementary insights to simulation-based studies [1–3]. Musculoskeletal humanoids and limb systems driven by tendon-like actuators have been shown to support biologically meaningful experiments on motion generation, internal force transmission, and neural control hypotheses [4–8]. This dual perspective of using robots to learn about biology and using biology to design more adaptive robots has been emphasized in both biomimetic robotics and biomechanics [4,9].

A wide range of actuation technologies have been explored in robotics, including electric motors, hydraulic systems, smart-material actuators, and artificial muscles [10,11]. Electric motors are widely used due to their controllability and maturity, but are limited by thermal constraints, gearing requirements, and reduced compliance compared to muscle-like actuators [12,13]. Hydraulic actuators offer exceptionally high power density and have enabled highly dynamic legged systems, but they remain relatively heavy, less efficient than biological muscle, and require a dedicated fluid infrastructure [13]. Dielectric elastomer actuators (DEAs), a class of electronic electroactive polymers, demonstrate high specific work and good bandwidth in comparative studies [11]. However, they are limited by

Check for updates

Academic Editor: Gary M. Bone

Received: 2 March 2026
Revised: 14 April 2026
Accepted: 17 April 2026
Published: 22 April 2026

Copyright: © 2026 by the authors. Licensee MDPI, Basel, Switzerland. This article is an open access article distributed under the terms and conditions of the Creative Commons Attribution (CC BY) license.

the need for kilovolt-range driving voltages [14], electromechanical instability, and the requirement for compliant electrodes [11]. In contrast, McKibben-style braided pneumatic actuators (BPAs) combine low mass, high force-to-weight ratio, and intrinsic compliance with a force–length curve that qualitatively resembles that of skeletal muscle [11,15]. BPAs have been used in quadrupedal robots [15,16], musculoskeletal humanoids [4,6], and dexterous manipulation systems [8], demonstrating their ability to support biologically motivated investigations and improve robot adaptability in unstructured environments.

Despite these advantages, BPAs exhibit several important differences from biological muscle. First, BPA maximum tensile force occurs at resting (i.e., uninflated) length (l_{rest}) rather than at an optimal fiber length [11]. Second, their maximum contraction ratio is substantially lower than that of human muscle, presenting challenges for achieving biomimetic joint ranges of motion [11,15,17]. Third, BPAs have a highly nonlinear dependence on internal pressure (P), contraction (ϵ), and loading state [15,18], which complicates control and motivates high-fidelity force–length–pressure modeling.

To address these challenges, numerous researchers have proposed static and dynamic models for BPAs. Sárosi et al. [17] compared geometric and empirical models for uninflated diameters (ϕ) 10 mm and 20 mm actuators and highlighted limitations when l_{rest} varies. Martens and Boblan [18] introduced a physically motivated static model for the Festo DMSP series and demonstrated accurate predictions at specific l_{rest}. Festo provides a manufacturer tool MuscleSIM for predicting force as a function of pressure and contraction [19], but experimental comparisons indicate that it does not adequately account for variation in l_{rest} or actuator-specific contraction limits. Hunt et al. [15] developed a more generalizable empirical model for ϕ10 mm Festo BPAs that incorporates differences between eccentric and concentric loading states and accounts for the maximum achievable contraction (ϵ_{max}) at high pressures. Comparisons with experimental data indicate that none of the existing models effectively take into account differences in maximum force due to initial actuator length.

The present work develops an improved force–pressure–length model for both ϕ10 mm and ϕ20 mm Festo BPAs. We collected extensive force data for a wide range of resting lengths, contraction ratios, and internal pressures. These data were first used to find maximum force as a function of resting length. Then we normalized the data to formulate normalized force (F^*) as a function of relative strain (ϵ^*) and relative pressure (P^*). The resulting model provides improved predictive accuracy for isometric BPA force, supporting the design and control of biomimetic robotic systems that rely on BPAs.

2. Background

Previous studies have generated empirical models of the force–length–pressure relationship of BPAs. Sárosi et al. [17] discuss several high-fidelity BPA force models. They present a static force model with a 21 coefficient polynomial function for a Festo MAS-20-200N (i.e., ϕ20 mm, $l_{rest} = 200$ mm) with an impressive $R^2 = 0.9994$. They also present Sárosi's static force model for a Festo DMSP-20-400N-RM-RM (i.e., ϕ20 mm, $l_{rest} = 400$ mm), with six coefficients and a $R^2 = 0.9995$. Martins and Boblan present an even more accurate model, in terms of absolute error, using five coefficients for a DMSP-10-250 (i.e., ϕ10 mm, $l_{rest} = 250$ mm) and a DMSP-20-300 (i.e., ϕ20 mm, $l_{rest} = 300$ mm) [18]. However, our work, as presented below, demonstrates that different resting lengths produce different force–length curves, preventing the use of these models for designing systems with different resting lengths.

Hunt et al. [15] looked at six resting lengths of ϕ10 mm Festo BPAs, accounting for differences in maximum contractile percentages, and elucidating the force–length–pressure relationship. In particular, for a given contraction percent and force F (in Newtons), the

scalar pressure P (in kPa) required to produce this force for a ϕ10 mm Festo artificial muscle can be determined by solving the equation:

$$P = 254\,\text{kPa} + F \cdot 1.23\,\text{kPa}\,\text{N}^{-1} + S \cdot 15.6\,\text{kPa} + 192\,\text{kPa} \cdot \tan\left(2.03\left(\frac{\epsilon}{\epsilon_{\max} - F \cdot 0.331 \times 10^{-3}\,\text{N}^{-1}} - 0.46\right)\right) \quad (1)$$

where S is the artificial muscle hysteresis factor such that $S = 1$ indicates the muscle is shortening, $S = -1$ indicates it is lengthening, and $S = 0$ under static conditions. An important note for Equation (2) is that the coefficients have been updated with the correct values as the values reported in [15] contained typographical errors. The amount of contraction, ϵ, is calculated as

$$\epsilon = \frac{(l_{rest} - l)}{l_{rest}} \quad (2)$$

where l is the current length of the BPA. ϵ_{max} in this case can also be described as ϵ_{620}, the amount of contraction in a BPA without external load when inflated at 620 kPa (90 psi), similarly calculated as

$$\epsilon_{620} = \frac{(l_{rest} - l_{620})}{l_{rest}} \quad (3)$$

where l_{620} is defined as the muscle length measured at 620 kPa. Equation (2) was used to create a lookup table for actuator force, F, for a given amount of pressure, P, and relative contraction, ϵ^*, defined as

$$\epsilon^* = \frac{\epsilon}{\epsilon_{620}} \quad (4)$$

using the results from Equations (2) and (3).

However, this model was taken with low external forces ($\leq$24 lbs), and it is unclear how well this model captures actuator behavior at higher forces, so we compare this model with data collected in this work.

3. Materials and Methods

3.1. Overview

To measure artificial muscle force as a function of length and pressure, we built a test jig from extruded alumnium and 3D printed parts. Festo BPAs with 10 mm and 20 mm diameter were tested with various resting lengths and different amounts of contraction. These data are used to develop an improved model that more accurately predicts maximum muscle force based on l_{rest}, current muscle length l_m, and pressure P. The results are compared with existing models and the new data are used to create an updated model.

3.2. BPA Force Characterization Experiment

A test jig was made of 80/20® brand 1515 series extruded aluminum (Figure 1). Artificial muscles were placed vertically in the jig one at a time. The upper end was attached to an load cell. Force data was collected using a CALT DYLY-103 100 kg S-shaped load cell for the ϕ10 mm BPAs and a Loadstar RAS1-2HKS-S for the ϕ20 mm BPAs. The was load cell was used in conjunction with a HX711 Load Cell Amplifier. Pressure data was obtained from a Freescale MPX5700 GP 5 V pressure sensor. Building air supply pressure was controlled with two pressure regulators in series. The first was a Parker model 20R113GC 0–120 psi pressure regulator. The second was a Husky 3/8 in. High Performance Air Regulator HDA72200. A Festo VTUG-10-MRCR-S1T-26V20-T516LA-UL-532S-8K valve manifold VTUG-G was used to deliver air from the pressure regulator to the actuator. This manifold is comprised of eight two-in-one bidirectional normally closed Festo VUVG-S10-T32C-AZT-M5-1T1L valves.

Pressure and load cell amplifier data were sent to Matlab 2021b via an Arduino Uno style Sparkfun BlackBoard C microcontroller. The computers that used Matlab were running either Windows 10 or Windows 11. During phases when the Arduino was collecting force and pressure data to send to Matlab, the Arduino would also trigger (via Matlab) an Onsemi 2N4401 NPN transistor to make the valve manifold open or close the valve. For other data collection, the valve was manually opened and closed.

The inner distance between the hose clamps on each BPA was measured with a FANUC tape measure to determine the muscle's length l and resting length (l_{rest}). This is how Festo AG & Co. KG [20] defines l_{rest}, although in Hunt et al. [15] it was measured to also include end cap length. We then inflated each BPA to $P_{620} = 620$ kPa, with one end allowed to move freely in the axial Degree of Freedom (DoF), and measured the length l_{620} to calculate maximum contraction at 620 kPa using Equation (3). The distance between the crossmembers was then controlled to obtain different amounts of contraction, the muscles were inflated to various pressures, and the contractile force was recorded at the pressure–contraction pairs. This was done for ϕ10 mm BPA resting lengths (l_{rest}) of 112 mm–518 mm. For ϕ20 mm BPAs, resting lengths (l_{rest}) of 300 mm–509 mm were used.

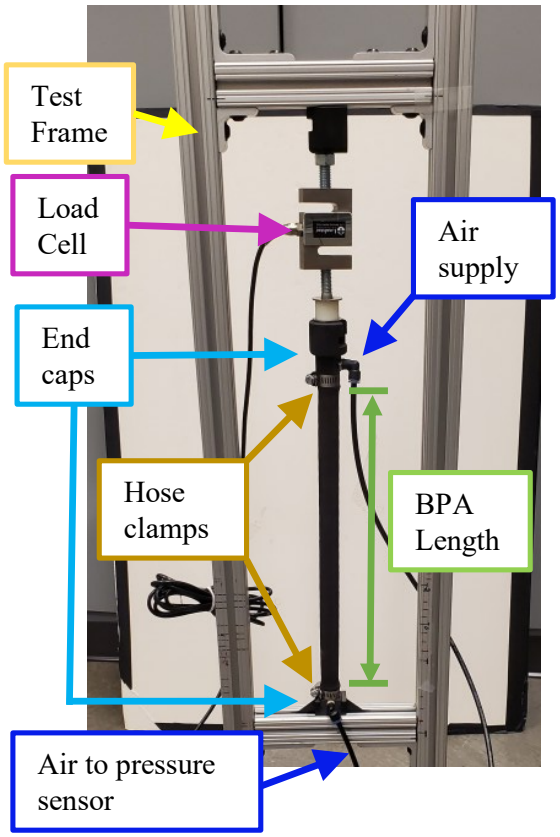


Figure 1. A picture of a BPA in the isometric force test stand with components labeled.

4. Results

4.1. Maximum Force at 620 kPa

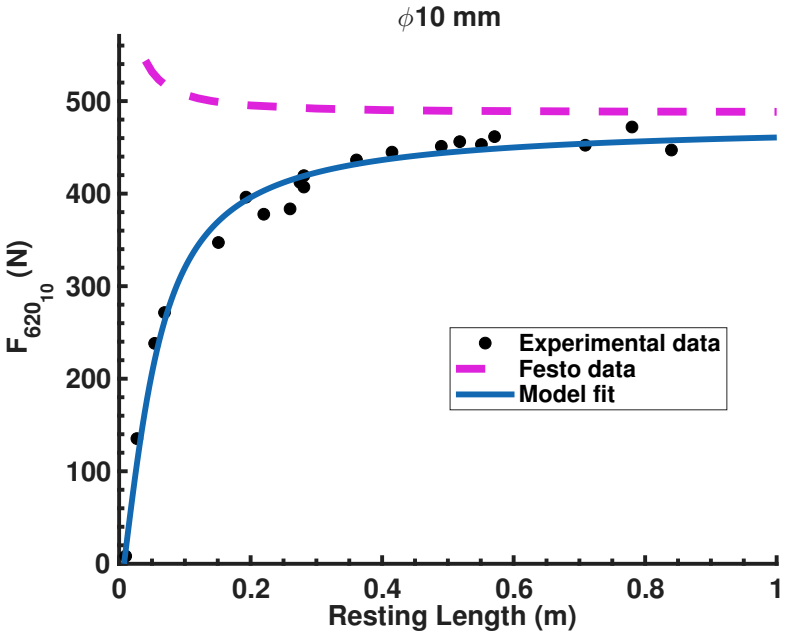
Data of the maximum force from BPA characterization tests of the 10 mm and 20 mm diameters at 620 kPa show a dependency on resting length (Figure 2). This is a previously unreported characteristic of these artificial muscles. Detailed analysis of the Festo tool [20] does in fact predict a change in maximum force with the resting length; however, the Festo tool predicts increased force with shorter lengths, while our collected data indicate decreasing force with shorter lengths. The data show a force response resembling an arctan

curve along the l_{rest} dimension. Using the Nonlinear Least Squares method and a Least Absolute Residual robustness, we fit an arctan curve to the data to get the maximum force at 620 kPa given a resting length as:

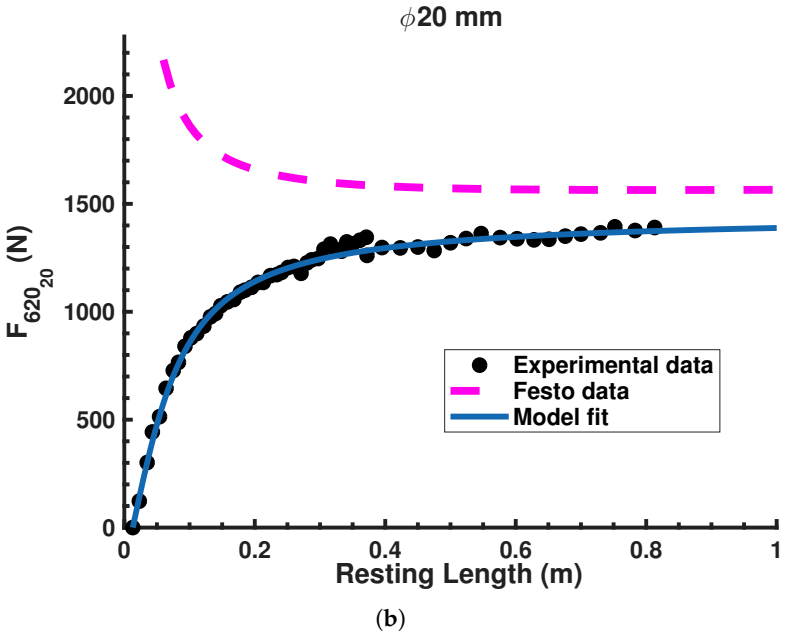
$$F_{620_{10}} = 303.5\,\text{N} \cdot \arctan\left(19.03\,\text{m}^{-1} \cdot (l_{rest} - 0.0075)\right) \quad (5)$$

$$F_{620_{20}} = 922.4\,\text{N} \cdot \arctan\left(15.37\,\text{m}^{-1} \cdot (l_{rest} - 0.013)\right) \quad (6)$$

The length is offset by 0.0075 m and 0.013 m because solid modeling showed that the end caps contact each other at these lengths. At these lengths, the actuator would not be able to contract to produce force.



(**a**)



(**b**)

Figure 2. Results for finding the relationship between F_{620} and l_{rest}. (**a**) $F_{620_{10}}$ as a function of l_{rest}, at P_{620}. Dashed line is the $F_{620_{10}}$ data from Festo. Solid line is the fit from Equation (5). (**b**) $F_{620_{20}}$ as a function of l_{rest} at P_{620}. Dashed line is $F_{620_{20}}$ data from Festo. Solid line is the fit from Equation (6).

4.2. Force as a Function of Pressure and Resting Length

Data from BPA characterization tests of the 10 mm muscles resulted in force–pressure pairings for different muscle resting lengths (l_{rest}) (Figure 3a). Similar to the maximum force data, these data show a force response resembling an arctan curve along the l_{rest} dimension with a more linear response to changes in pressure. Using the Nonlinear Least Squares method and a Least Absolute Residual robustness, we fit an arctan curve to the data to get the maximum force given a resting length and pressure as:

$$F_{max}(l_{rest}, P) = a_1 \cdot P \cdot \arctan\left(a_2 \cdot P \cdot (l_{rest} - 0.0075)\right) \tag{7}$$

where $a_1 = 0.4895\,\mathrm{N\,kPa^{-1}}$ and $a_2 = 0.030\,68\,\mathrm{kPa^{-1}\,m^{-1}}$ for the 10 mm actuator, and $a_1 = 1.49\,\mathrm{N\,kPa^{-1}}$, $a_2 = 0.0248\,\mathrm{kPa^{-1}\,m^{-1}}$ for the 20 mm actuator. Goodness-of-fit measures are given in Table 1.

Table 1. Maximum force equation coefficient values with confidence intervals (CI) and goodness-of-fit measures. Equation (7) is compared to data taken at 620 kPa . Equations (5) and (6) are compared against maximum force from using the Festo tool. It was not necessary to fit an adjusted R^2 in these cases.

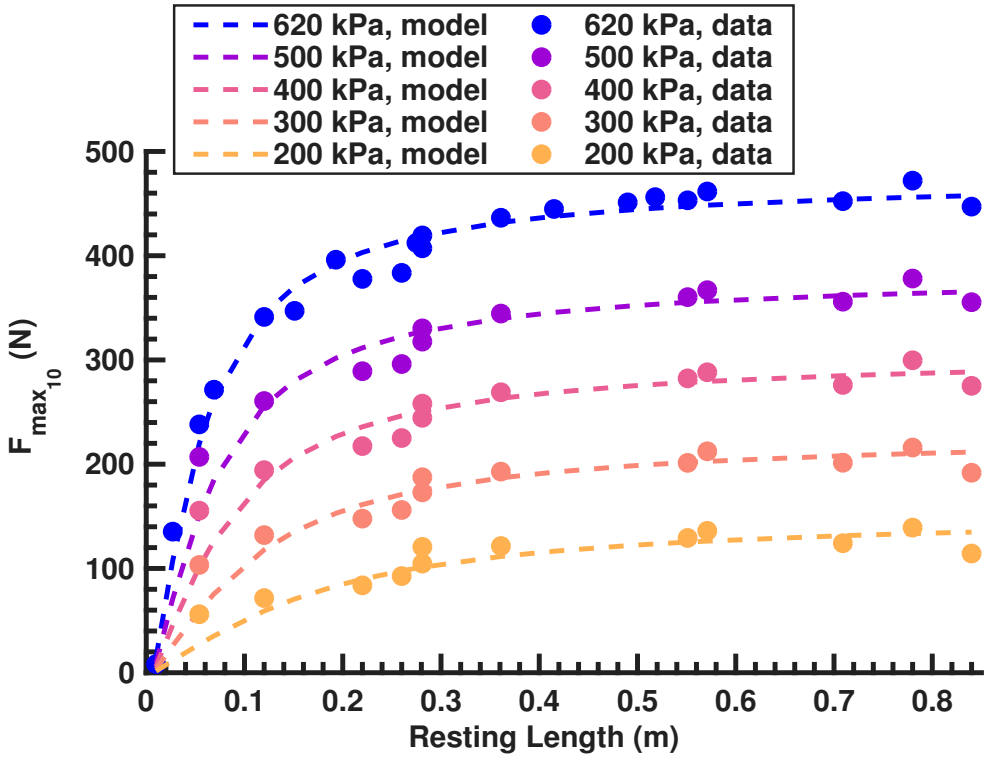
Equation	Coefficient	CI (95%)	Our Model			Festo Tool		
			Adj. R^2	RMSE	Max. Error	Adj. R^2	RMSE	Max. Error
(7)	$a_1 = 0.4895\,\mathrm{N\,kPa^{-1}}$ $a_2 = 0.030\,68\,\mathrm{kPa^{-1}\,m^{-1}}$	(0.4822, 0.4968) (0.0282, 0.03317)	0.9945	11.61 N	55.3 N	0.9854	14.7 N	30.9 N
(5)	$b_1 = 303.5\,\mathrm{N}$ $b_2 = 19.03\,\mathrm{m^{-1}}$	(300, 308) (17.48, 20.57)	0.9854	14.72 N	30.9 N	–	189.9 N	375.6 N
(6)	$b_1 = 922.4\,\mathrm{N}$ $b_2 = 15.37\,\mathrm{m^{-1}}$	(914.2, 930.7) (14.75, 15.98)	0.9945	23.83 N	62.1 N	–	668.4 N	1590.1 N

4.3. Maximum Contraction at 620 kPa

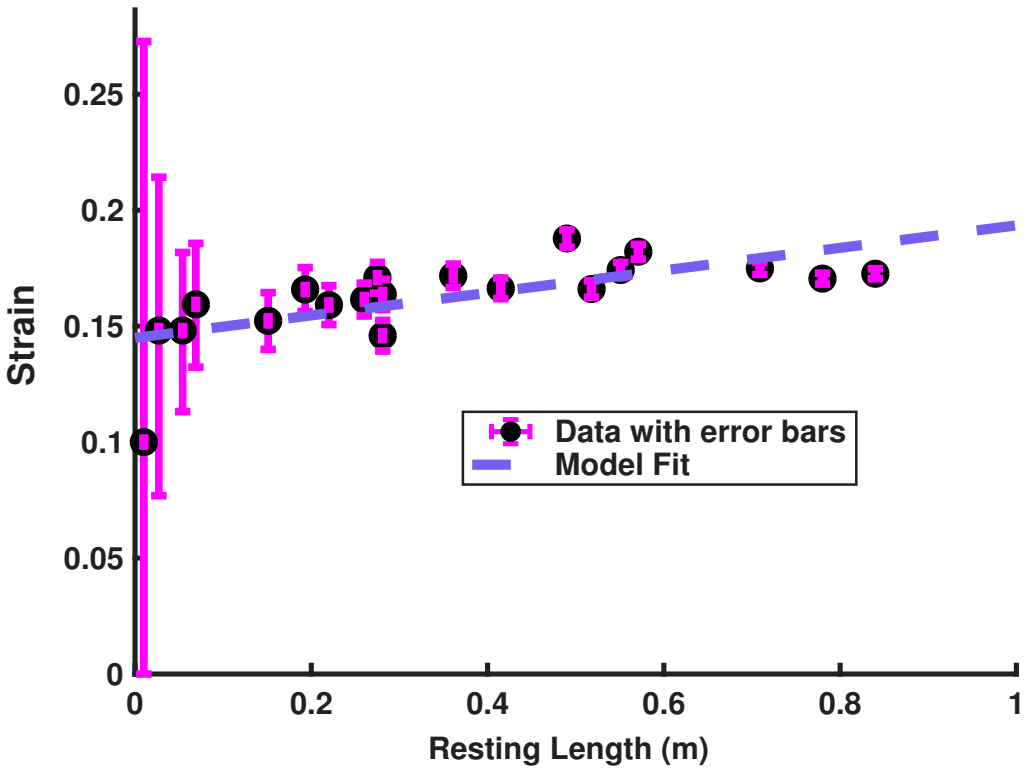
Figure 3b shows an attempt at a linear fit for maximum contraction at 620 kPa (ϵ_{620}) as a function of resting length (l_{rest}). Error bars have been included to show the effect of ± 1 mm accuracy with measurements of l_{rest} and l_{620}. There was a large amount of variance in the data, with the linear fit giving an adjusted $R^2 = 0.4124$ and an RMSE $= 0.0083$. Since there is no direct, predicable relationship between maximum contraction and l_{rest}, this value should be recorded in each muscle used on a robot to best predict the force it may produce at different pressures and contraction.

4.4. Force as a Function of Pressure and Contraction

In addition to being a function of the pressure and resting length, the force produced by the actuator is also a function of the amount of actuator contraction, with less force being applied as the actuator contracts. To build this model, the collected data of force, pressure, and contraction are normalized by dividing by F_{620}, P_{620}, and ϵ_{620}, respectively. This had the effect of compressing the data into a 3D surface ranging from 0 to 1 on all axes. Normalized data are compared with pressure isoclines of force predicted by the Festo tool divided by the maximum force equation described in the previous section in Figure 4. With this comparison, it is clear that the Festo tool over-predicts the expected force, especially at lower pressures, contraction, and resting lengths.

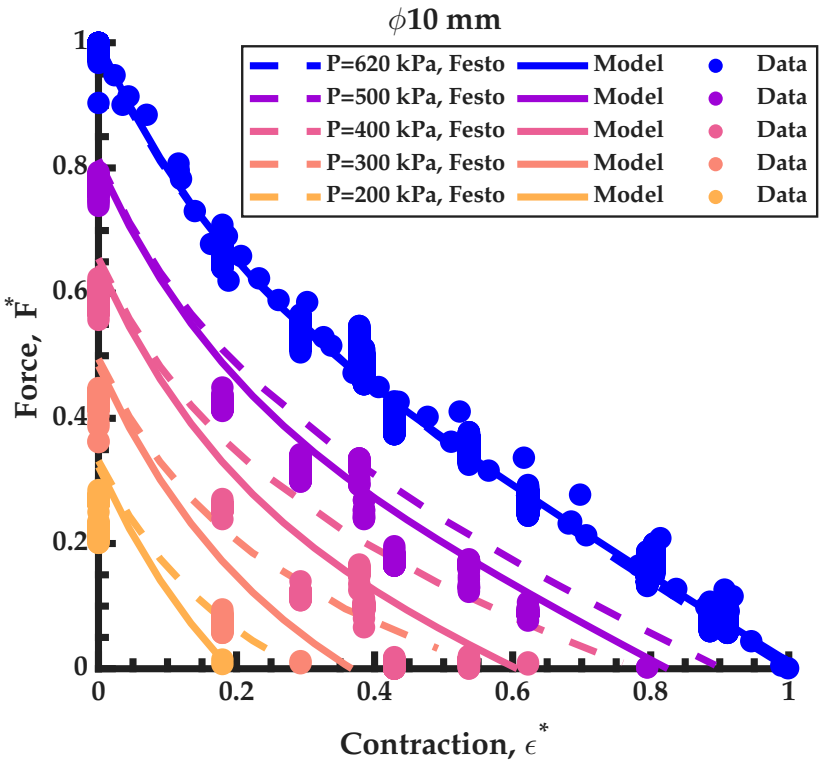


(**a**)

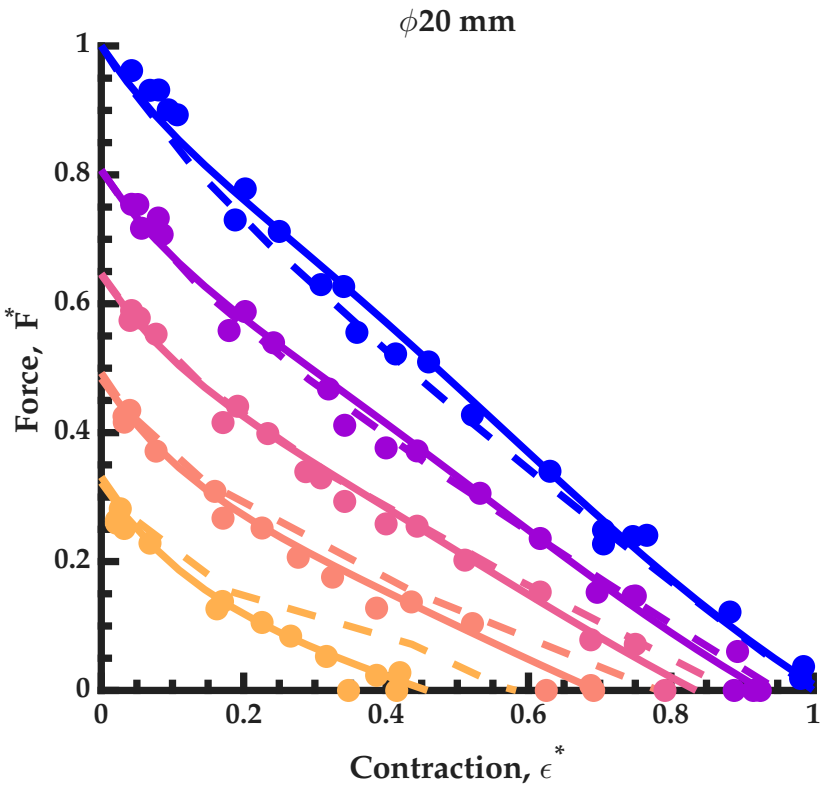


(**b**)

Figure 3. Results for finding the relationship between F_{620}, l_{rest}, P_{620}, and $\epsilon_{620_{10}}$. (**a**) Isoclines of the surface fit for $F_{620_{10}}(l_{rest}, P_{620})$. (**b**) $\epsilon_{620_{10}}$ versus l_{rest} at P_{620}. Although there is a general trend of longer resting lengths producing more contraction, no conclusive relationship between ϵ_{620} and l_{rest} could be deduced from this experiment. The error bars show the effect of being ± 1 mm in measuring l_{rest} and l_{620}.



(**a**)



(**b**)

Figure 4. Surface fit for $F^*(\epsilon^*, P^*)$. Solid lines are from our model. Dashed lines from Festo supplied data. In total, 537 data points were collected and used to fit the 3D surfaces (321 data points for ϕ10 mm BPAs and 216 data points for ϕ20 mm BPAs). In total, 80% of these data were used for training, and 20% were used for validation. For figure clarity, not all data is included and plotted circles represent collected data at $\pm$10 kPa of the stated pressure. (**a**) Fit data for ϕ10 mm Festo BPAs. (**b**) Fit data for ϕ20 mm Festo BPAs.

We therefore derived our own equation for isometric force in the BPA as a function of pressure and contraction. Visual analysis of the experimental data shows an exponential relationship between ϵ^* and F^*, and a linear relationship between P^* and F. We fit a surface to the data using Nonlinear Least Squares and a Least Absolute Residual robustness such that:

$$F^*(\epsilon^*, P^*) = \begin{cases} c_0 \cdot \left(\exp(-c_1 \cdot \epsilon^*) - 1\right) + P^* \cdot \exp(-c_2(\epsilon^*)^2) & \text{for } F^* > 0 \\ 0 & \text{for } F^* \leq 0 \end{cases} \quad (8)$$

For the ϕ10 mm BPAs, the result of the improved fit can be seen in Figure 4a. The adjusted $R^2 = 0.9998$, a RMSE $= 0.004537$, and a maximum absolute residual of 10.6%. Solving (8) for the ϕ20 mm BPA, yields different coefficients, and results are seen in Figure 4b. Coefficient values and goodness-of-fit statistics are found in Table 2.

Table 2. Normalized isometric BPA force equation (Equation (8)) coefficient values and goodness-of-fit measures.

BPA	Coefficient	CI (95%)	Model			Validation		
			Adj. R^2	RMSE	Max. Error	Adj. R^2	RMSE	Max. Error
ϕ10 mm	$c_0 = 0.5682$	(0.5584, 0.578)	0.9998	0.005118	10.3%	0.9994	0.0245409	10.6%
	$c_1 = 4.254$	(4.126, 4.383)						
	$c_2 = 0.5597$	(0.5429, 0.5766)						
ϕ20 mm	$c_0 = 0.2579$	(0.2401, 0.2756)	0.992	0.02294	6.8%	0.9943	0.0231303	5.7%
	$c_1 = 6.477$	(5.558, 7.396)						
	$c_2 = 1.321$	(1.239, 1.403)						

5. Discussion

5.1. Effects of Resting Length

We have developed new F_{620} equations for 10 mm and 20 mm diameter Festo BPAs that capture the change in maximum force produced by the actuators at 620 kPa as a function of their resting length. When examining Equation (5) and measured data in Figure 2b, it can be seen that as l_{rest} goes to infinity, $F_{620_{10}}$ goes to 470 N. When the Festo tool [19] was queried at $l_{rest} = 1$ m as an approximation of infinity, it predicts the ϕ10 mm BPA can produce $F = 490$ N at P_{620}. This is within the 10% variability that Festo states may occur in manufacturing tolerances. Similarly, the Festo data predict a ϕ20 mm BPA will produce $F = 1570$ N. Our results for Equation (6) show that $F_{620_{20}}$ goes to 1460 N as l_{rest} approaches infinity. Although the difference is much larger, it is also with the 10% manufacturing tolerance.

Where our measured data differs significantly from the Festo model, is that as l_{rest} goes to zero. For the measured data, as the length gets smaller, the force does as well, whereas the Festo tool predicts exponential force increase (see Figure 2). As a specific example, when specifying $l_{rest} = 112$ mm for the 10 mm diameter BPAs, the Festo predicted F_{620} is 498.6 N. However, using Equation (5), F_{620} is calculated to be 335.3 N. Actual force in the $l_{rest} = 112$ mm was measured at 350.9 N Therefore, the error in predicted F_{620} for the ϕ10 mm BPA is 4.5% for our model and 42.1% using the Festo tool. Researchers using BPA resting lengths under 300 mm should take note of these results.

Festo AG & Co. KG [20] (p. 12) states that force will be reduced by approximately 10% for a minimum nominal length. In Festo AG & Co. KG [21] (p. 14) they say the force can deviate by 10% based on factors such as: production variation, material variation, and

deviation from nominal length (l_{rest}). Festo AG & Co. KG [22] (p. 13) notes that testing was done with BPAs that are ten times the uninflated diameter, and that theoretical force can increase by up to 10%. In each datasheet, the characteristic curves appear to be the same. As demonstrated above, the 100 mm ϕ10 mm BPA should have much less force than what is shown in the curve. This is our experience and the reason for the testing. It is unclear why the MuscleSIM tool [19] then predicts higher force as resting length decreases. It could be a reversed sign coefficient in their internal curve-fit model. We have shown here that as the nominal length goes to zero, so does force.

The reason for BPA models predicting higher force than what is measured experimentally is a recurrent theme across many models: they do not account for the end effects of the pressure vessel where end effects dominate. Nominally, the clamped ends fix the inner and outer diameter while allowing axial and radial displacement. In the isometric case, there is only radial displacement. The boundary conditions force steep gradients in stress and strain near the ends. Near the boundary conditions are where axial, radial, and circumferential strains deviate from analytic solutions to a cylindrical model. For a constant pressure, the end effect region appears to have the same length. Therefore, in shorter BPAs, the end effects dominate. The axial length scale of the boundary section is comparable to l_{rest}, and the active force differs substantially from that of an assumed perfect cylinder.

Manufacturing variations seem to play an important factor in the behavior of these actuators. It remains to be seen how ϵ_{620} can be known a priori. We still suspect that it is a function of l_{rest}, but it might also be a function of other factors such as product batch number or UV light exposure [20] (p. 15); [21] (p. 6); [22] (p. 13). We found there to be larger variations in the 10 mm BPAs than in the 20 mm BPAs. Modeling work of ideal McKibben actuators describe how the relationship between contraction and initial length is a function of the total number of twists and the angle of twist in the usable muscle area [23]. It is unclear if there are variations in the angle and number of twists in the Festo BPAs due to manufacturing. Uncovering the relationship between ϵ_{620} and l_{rest} for the Festo DMSP artificial muscles, if it exists in a meaningful way, will require additional controlled tests.

Similarly, it is not clear how the maximum force might change with manufacturing variations. This was reasonably corrected for by normalizing the equations to each individual's maximum contraction, but more nuanced details might emerge with more data collection. Not knowing these relationships a priori means there is still a need for robots and other systems to go through an iterative design stage if it is discovered that the system does not produce the torque or have the RoM that the design team expects. However, the data and models provided here should enable for faster redesigns with fewer additional measurements.

5.2. Nondimensionalization

We have also introduced the concept of nondimensionalized isometric force that is a function of relative strain and relative pressure (Equation (8)). This elegant equation has only three coefficients with low error (see Table 2). In the work presented here, we introduce the relative pressure term, $P^* = P/P_{620}$. Our data show that by normalizing force, contraction, and pressure, we are able to create a simplified force equation as a function of contraction and pressure that scales well with initial actuator length, i.e.,

$$F(\epsilon^*, P^*, l_{rest}) = F^*(\epsilon^*, P^*) \cdot F_{620}(l_{rest}) \tag{9}$$

For example, given $l_{rest} = 54$ mm and $P = 300$ kPa, the measured force was $F_{actual} = 103$ N. Force prediction using only the Festo tool predicts the force to be $F_{predict} = 270$ N. This is 161% greater than the measured force. Using Equations (5) and (8)

with Equation (9) gives $F_{predict} = F^*(0, 0.48) \cdot F_{620}(0.054) = 0.49 \cdot 230\,\text{N} = 112\,\text{N}$. This is an error of 8%, which is much more accurate than using the Festo tool only.

The presented work is capable of predicting force output for 10 mm and 20 mm muscles with different initial muscle lengths, internal pressure, and contraction amount with minimal initial data collection. However, it remains to be seen if these relationships are maintained over the full lifecycle of the muscles. There are not yet any peer reviewed studies investigating the long-term behavior of these artificial muscles, though the Festo datasheet provides some indication of what can be expected [20] (p. 19). They report that the 40 mm BPA can complete 1 million cycles at 6000 N (maximum rated load), or 10 million cycles at 4000 N. The service life of the other size BPAs is not reported; however, it is mentioned that thermal stressing may reduce the lifespan and they should be inspected every 500,000 cycles for signs of aging [21] (pp. 10–11). Future research should look at the behavior of these muscles over time.

In our work, $P_{620} = 620$ kPa is the maximum supply pressure for our system, and other users of this actuator may use a different supply pressure. However, this supply pressure is not required, and normalizing by this value was chosen as a method for improving the optimization techniques by reducing the sensitivity of the term associated with pressure. This equation will work for any pressure supplies below 620 kPa. We also anticipate the equation will also work for pressures up to 800 kPa (the maximum rated pressure for Festo ϕ10 mm BPAs); however, we do not have the data to confirm this.

5.3. Comparison with Other Published BPA Models

The proposed model was compared with the formulations by Sárosi [24], Sárosi and Fabulya [25], and Martens and Boblan [18], to evaluate their predictive performance across actuator sizes and operating conditions (see Table 3 and Figure 5). For the ϕ20 mm BPA, parameters from [24] were used, corresponding to actuators with resting lengths of 200 mm and 400 mm. These were compared against the experimental data at $l_{rest} = 300$ mm and $l_{rest} = 450$ mm, respectively. For the ϕ10 mm BPA with resting lengths of 257 mm and 233 mm, parameters from [25] were applied. In each case, the maximum contraction parameter (k_{max}) was determined numerically by solving $F(6.2\,\text{bar}, k_{max}) = 0$, ensuring consistency with the experimental maximum pressure condition.

Table 3. Goodness-of-fit comparison for the Bolen, Sárosi, and Martens and Boblan models at different resting lengths (in mm) for 10 mm and 20 mm BPAs. RMSE and maximum error are reported in newtons, and FVU denotes the fraction of variance unexplained.

Diameter	Length	Bolen			Sarosi			Martens and Boblan		
		RMSE	FVU	Max. Error	RMSE	FVU	Max Error	RMSE	FVU	Max. Error
10 mm	257	22.9	0.0353	46.0	143.8	1.3903	235.8	73.8	0.3668	122.9
	233	16.8	0.0187	30.3	132.7	1.1655	222.6	62.6	0.2590	101.2
20 mm	300	35.6	0.0144	114.0	132.1	0.1992	313.4	72.8	0.0605	137.8
	450	67.6	0.0258	166.6	177.7	0.1785	294.8	862.1	4.2022	1321.1

While the Sárosi [24] and Sárosi and Fabulya [25] models capture general trends in force–contraction behavior, discrepancies were observed when applying parameters derived from different actuator lengths. In particular, the model tends to over-predict force at higher pressures and low amounts of contraction, suggesting sensitivity to geometric scaling effects not explicitly accounted for in the formulation.

The Martens and Boblan [18] model is derived from a geometric and material-based framework and provides a more physically grounded representation of actuator behavior. However, its accuracy depends strongly on precise geometric parameters, including braid

angle, wall thickness, and fiber length. Small deviations in these parameters can lead to significant differences in predicted force, particularly at higher pressures.

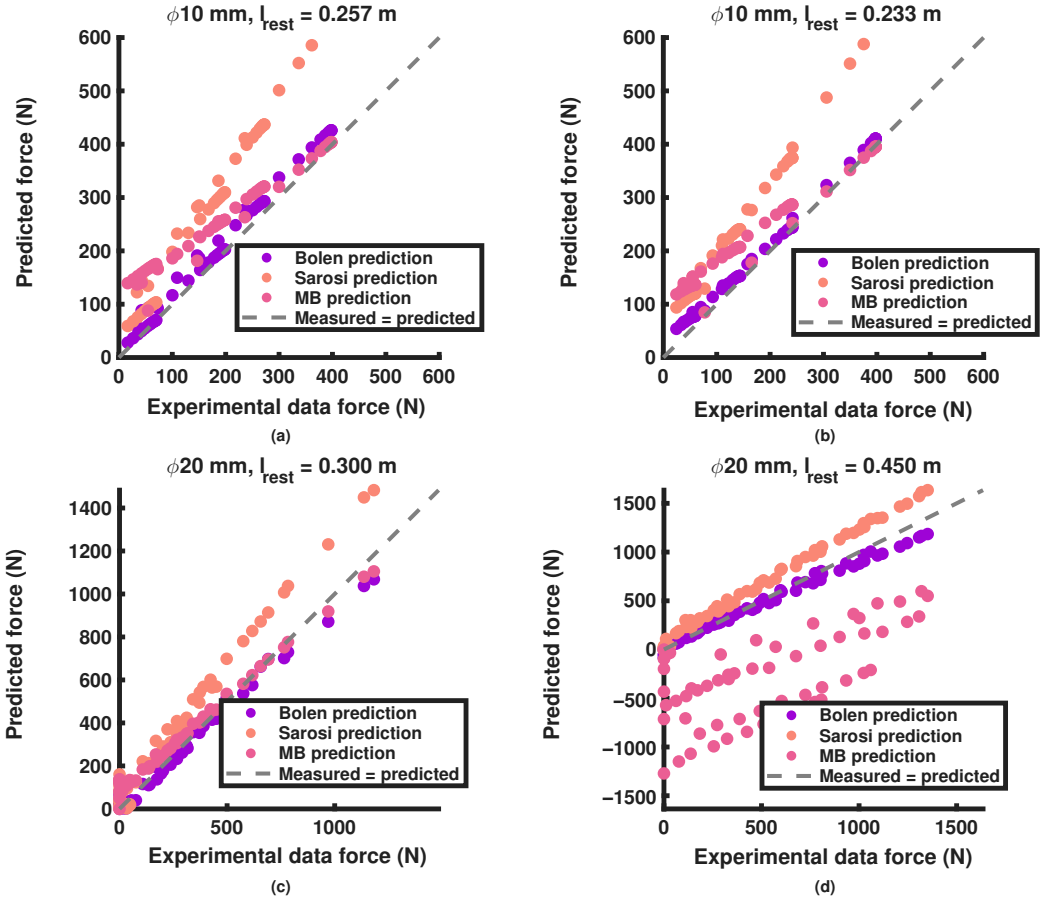


Figure 5. Comparison between measured and predicted BPA force at varying amounts of contraction and pressure. A $y = x$ perfect fit line is added for reference. The BPAs compared are: (**a**) ϕ10 mm, l_{rest} = 0.257 mm, (**b**) ϕ10 mm, l_{rest} = 0.233 mm, (**c**) ϕ20 mm, l_{rest} = 0.300 mm, and (**d**) ϕ20 mm, l_{rest} = 0.450 mm.

The Martens and Boblan model was first evaluated at the same pressure–contraction points as in their experimental data [18] (Tables A1 and A2), indicating that it reproduces the general published force map shape but is sensitive to the assumed initial geometry. Examining their ϕ20 mm BPA, for example, using the explicitly stated l_{rest} = 300 mm and initial diameter D_0 = 20 mm significantly under-predicted the results compared to using the implied l_{rest} = 296 mm ([18] (Table A1)) and $D_0 + H_0$ = 21.8 mm, where H_0 = 1.8 mm is the material thickness. The diameter adjustment can be implied from [23]. This adjusted diameter was also included for the ϕ10 mm BPA to give a better fit. As can be seen in Figure 5 and Table 3, the highest accuracy is observed when ϕ20 mm and l_{rest} = 300 mm, which is at or very near their experimental measurements. For the ϕ10 mm BPAs the accuracy decreases even though their experimentally measured l_{rest} = 250 mm is close to our l_{rest} = 257 mm and l_{rest} = 233 mm. The largest error occurs at ϕ20 mm and l_{rest} = 450 mm and the model starts to predict negative force. We have calculated that the $F_{PE} \cdot \frac{dD}{DL}$ term becomes very large compared to the others [18] (p. 5). This suggests that the model is sensitive to geometric parameter selection and interpretation, particularly with respect to initial length and diameter definitions.

In comparison, the present normalized model demonstrates improved consistency across actuator lengths by incorporating experimentally derived scaling through F_{620} and ϵ_{620}. This normalization reduces sensitivity to geometric variation and enables a unified

representation of actuator behavior, while maintaining predictive accuracy over the tested range of pressures and contractions.

5.4. Implications for Real-Time Control and Simulation

Although pneumatic muscle actuators exhibit hysteresis, thermodynamic effects, and other dynamic behavior, accurate and high-performance controller designs can still be achieved using a static force map approach when the underlying static force model is accurate. Martens and Boblan explicitly note that BPA dynamics are often dominated by the air dynamics inside the actuator and the mass flow behavior of the valve, such that precise modeling of the static force characteristic remains crucial for torque control accuracy [18]. This view is consistent with more recent BPA control work, including a sensor-less torque control interface for BPA-driven joints [26], stable force/position/stiffness control of antagonistic pneumatic-muscle joints [27,28], and sensor-less angle stiffness control of antagonistic BPA systems [29].

In this context, the present model is well suited for real-time use because it reduces the static isometric force prediction to a low-order normalized surface, $F^*(\epsilon^*, P^*)$, scaled by the resting-length-dependent term $F_{620}(l_{rest})$. This structure is computationally inexpensive to evaluate online and is also suitable for lookup-table implementation. While the present work does not model the full actuator–valve dynamics, it provides the static force relationship needed as a feedforward or inner-model component in real-time torque control, simulation, and preliminary design workflows. It is anticipated that improved real-time control for high-speed and high-precision systems will benefit more from improved modeling of airflow dynamics than dynamics involving actuator hysteresis, damping, and other dynamic behavior.

5.5. Biomimetic Artificial Muscle Analogy

BPA artificial muscles are often said to be analogous to biological muscles because they have force–length curves and can produce force only in tension. This analogy is worth closer inspection. For example, the describes the passive force–length curve has been described as an exponential function arising from connective tissue elements, while the active force–length relationship is typically modeled as a bell-shaped curve reflecting actin–myosin overlap [30]. These formulations emphasize that muscle force generation is governed by nonlinear geometric and material interactions rather than simple linear elasticity. McKibben-type pneumatic artificial muscles (of which Festo is an example) exhibit analogous nonlinear behavior, though arising from fundamentally different physical mechanisms. As shown by Chou and Hannaford, the force–length relationship of McKibben actuators is derived from geometric constraints imposed by the braided shell, leading to a nonlinear dependence of force on actuator length through the braid angle [23]. In their formulation, actuator force is proportional to pressure and a nonlinear geometric term $(3\cos^2\theta - 1)$, which governs both the maximum contraction limit and the curvature of the force–length relationship. The work presented here demonstrates that this nonlinear curve can be well approximated by an exponential as well.

However, there are some distinct differences between how these artificial muscles behave when compared to biological muscles. For example, the biological muscle optimum fiber length l_{OFL} is not equivalent to l_{rest} in the muscles. The maximum active force that the artificial muscles can produce is at the resting length, also the maximum length, of the artificial muscles. In contrast, the maximum active force a biological muscle length can produce is somewhere in the middle of the total contractile length of the muscle.

Furthermore, biological muscles can adapt the optimal operating length through structural remodeling (e.g., sarcomere addition or tendon compliance) while BPAs have

a fixed geometric configuration. This allows biological systems to self-optimize for the particular tasks the animal is subjected to. In order to re-optimize a robot for new tasks, new actuators would have to be swapped into the system. This distinction highlights a key limitation of BPAs in biomimetic applications, while also reinforcing the importance of accurate nonlinear modeling for control and design.

6. Conclusions

The analysis in this study has created novel equations for calculating force in Festo 10 mm and 20 mm diameter BPAs. This study has elucidated the relationship between maximum BPA force at 620 kPa F_{620} as a function of resting length l_{rest} (Equations (5) and (6), Table 1). We have also created more accurate equations for the nondimensionalized force in a BPA as a function of relative strain ϵ^* and relative pressure P^*, (Equation (8) and Table 2). Taken together, the $F_{620}(l_{rest})$ fits and the nondimensional force surface $F^*(\epsilon^*, P^*)$ provide a practical way to predict isometric BPA force across resting lengths using a small number of measurements. In a design workflow, these equations make it easier to select actuator diameter and resting length, and to evaluate whether a proposed routing can meet force and range-of-motion requirements before committing to a full prototype. As a result, BPA-driven mechanisms (e.g., joints in biomimetic legs or manipulators) can be developed with fewer design iterations and with realistic expectations of force output at short resting lengths.

Author Contributions: Conceptualization, B.B. and A.H.; Methodology, B.B., A.H., M.E. and L.P.; Software, B.B., M.E. and L.P.; Validation, B.B. and A.H.; Formal Analysis, B.B.; Investigation, B.B., M.E. and L.P.; Resources, B.B. and A.H.; Data Curation, B.B. and L.P.; Writing—Original Draft Preparation, B.B.; Writing—Review and Editing, B.B., M.E., L.P. and A.H.; Visualization, B.B. and A.H.; Supervision, B.B. and A.H.; Project Administration, B.B. and A.H.; Funding Acquisition, A.H. All authors have read and agreed to the published version of the manuscript.

Funding: Research for this article was funded by the Department of Mechanical and Materials Engineering at Portland State University, the National Science Foundation (NSF) grant for NeuroNex: Communication, Coordination, and Control in Systems (C3NS) 2015317 and NSF grant 1943483.

Institutional Review Board Statement: Not applicable.

Informed Consent Statement: Not applicable.

Data Availability Statement: The data sets are available from the authors upon reasonable request.

Acknowledgments: The authors would like to thank Jasmine Bradley for her help reworking the figures in the results and discussion sections. As a visual designer, her contributions improved the aesthetic quality of the images and ensured data accessibility for people with color blindness. Furthermore, the authors would like to express their gratitude towards Cody Scharzenberger for all his assistance in proof-reading and editing the manuscript.

Conflicts of Interest: The authors declare no conflicts of interest. The funders had no role in the design of the study; in the collection, analyses, or interpretation of data; in the writing of the manuscript; or in the decision to publish the results.

Abbreviations

The following abbreviations are used in this manuscript:

BPA Braided Pneumatic Actuator

References

1. Andrews, J.G. A General Method for Determining the Functional Role of a Muscle. *J. Biomech. Eng.* **1985**, *107*, 348–353. [CrossRef]
2. Millard, M.; Uchida, T.; Seth, A.; Delp, S.L. Flexing Computational Muscle: Modeling and Simulation of Musculotendon Dynamics. *J. Biomech. Eng.* **2013**, *135*, 021005. [CrossRef]
3. Arnold, E.M.; Ward, S.R.; Lieber, R.L.; Delp, S.L. A Model of the Lower Limb for Analysis of Human Movement. *Ann. Biomed. Eng.* **2010**, *38*, 269–279. [CrossRef]
4. Asano, Y.; Okada, K.; Inaba, M. Design principles of a human mimetic humanoid: Humanoid platform to study human intelligence and internal body system. *Sci. Robot.* **2017**, *2*, eaaq0899. [CrossRef]
5. Asano, Y.; Okada, K.; Inaba, M. Musculoskeletal design, control, and application of human mimetic humanoid Kenshiro. *Bioinspir. Biomim.* **2019**, *14*, 036011. [CrossRef]
6. Hitzmann, A.; Masuda, H.; Ikemoto, S.; Hosoda, K. Anthropomorphic musculoskeletal 10 degrees-of-freedom robot arm driven by pneumatic artificial muscles. *Adv. Robot.* **2018**, *32*, 865–878. [CrossRef]
7. Liu, X.; Rosendo, A.; Ikemoto, S.; Shimizu, M.; Hosoda, K. Robotic investigation on effect of stretch reflex and crossed inhibitory response on bipedal hopping. *J. R. Soc. Interface* **2018**, *15*, 20180024. [CrossRef] [PubMed]
8. Chen, J.; Zhong, S.; Kang, E.; Qiao, H. Realizing human-like manipulation with a musculoskeletal system and biologically inspired control scheme. *Neurocomputing* **2019**, *339*, 116–129. [CrossRef]
9. Ijspeert, A.J. Amphibious and Sprawling Locomotion: From Biology to Robotics and Back. *Annu. Rev. Control. Robot. Auton. Syst.* **2020**, *3*, 173–193. [CrossRef]
10. He, J.; Gao, F. Mechanism, Actuation, Perception, and Control of Highly Dynamic Multilegged Robots: A Review. *Chin. J. Mech. Eng.* **2020**, *33*, 79. [CrossRef]
11. Liang, W.; Liu, H.; Wang, K.; Qian, Z.; Ren, L.; Ren, L. Comparative study of robotic artificial actuators and biological muscle. *Adv. Mech. Eng.* **2020**, *12*, 1687814020933409. [CrossRef]
12. Veale, A.J.; Xie, S.Q. Towards compliant and wearable robotic orthoses: A review of current and emerging actuator technologies. *Med. Eng. Phys.* **2016**, *38*, 317–325. [CrossRef] [PubMed]
13. Suzumori, K.; Faudzi, A.A. Trends in hydraulic actuators and components in legged and tough robots: A review. *Adv. Robot.* **2018**, *32*, 458–476. [CrossRef]
14. Madden, J.; Vandesteeg, N.; Anquetil, P.; Madden, P.; Takshi, A.; Pytel, R.; Lafontaine, S.; Wieringa, P.; Hunter, I. Artificial muscle technology: Physical principles and naval prospects. *IEEE J. Ocean. Eng.* **2004**, *29*, 706–728. [CrossRef]
15. Hunt, A.; Graber-Tilton, A.; Quinn, R. Modeling length effects of braided pneumatic actuators. In *ASME 2017 International Design Engineering Technical Conferences and Computers and Information in Engineering Conference. Volume 5A: 41st Mechanisms and Robotics Conference, Cleveland, OH*; American Society of Mechanical Engineers: New York, NY, USA, 2017; Volume 58172, p. V05AT08A008. [CrossRef]
16. Aschenbeck, K.; Kern, N.; Bachmann, R.; Quinn, R. Design of a Quadruped Robot Driven by Air Muscles. In *The First IEEE/RAS-EMBS International Conference on Biomedical Robotics and Biomechatronics, 2006. BioRob 2006*; IEEE: Piscataway, NJ, USA, 2006; pp. 875–880. [CrossRef]
17. Sárosi, J.; Piteľ, J.; Tóthová, M.; Hošovský, A.; Bíró, I. COMPARATIVE SURVEY OF VARIOUS STATIC AND DYNAMIC MODELS OF PNEUMATIC ARTIFICIAL MUSCLES. *Trans. Can. Soc. Mech. Eng.* **2017**, *41*, 825–844. [CrossRef]
18. Martens, M.; Boblan, I. Modeling the Static Force of a Festo Pneumatic Muscle Actuator: A New Approach and a Comparison to Existing Models. *Actuators* **2017**, *6*, 33. [CrossRef]
19. Lang, R. *MuscleSIM*, Version 2.0.1.5; Dept. TK-ES, Festo AG & Co. KG.: Esslingen am Neckar, Germany, 2005.
20. Festo AG & Co. KG. Fluidic Muscle DMSP. [Product Datasheet]. 2026. Available online: https://www.festo.com/media/catalog/202851_documentation.pdf (accessed on 26 March 2026).
21. Festo AG & Co. KG. Fluidic Muscle DMSP/MAS. [Product Datasheet]. 2018. Available online: https://www.festo.com/net/en_us/SupportPortal/Files/732773/DMSP_MAS_2018-01f_8081496g1.pdf (accessed on 26 March 2026).
22. Festo AG & Co. KG. Fluidic Muscle DMSP/MAS. [Product Datasheet]. 2013. Available online: https://ftp.festo.com/Public/PNEUMATIC/SOFTWARE_SERVICE/Documentation/2015/EN/DMSP-MAS_EN.PDF (accessed on 26 March 2026).
23. Chou, C.P.; Hannaford, B. Measurement and modeling of McKibben pneumatic artificial muscles. *IEEE Trans. Robot. Autom.* **1996**, *12*, 90–102. [CrossRef]
24. Sárosi, J. New approximation algorithm for the force of fluidic muscles. In *2012 7th IEEE International Symposium on Applied Computational Intelligence and Informatics (SACI)*; IEEE: Piscataway, NJ, USA, 2012; pp. 229–233.
25. Sárosi, J.; Fabulya, Z. Mathematical analysis of the function approximation for the force generated by pneumatic artificial muscle. *Sci. Bull. Politeh. Univ. Timiș. Trans. Mech.* **2012**, *57*, 59–64.
26. Martens, M.; Seel, T.; Zawatzki, J.; Boblan, I. A Novel Framework for a Systematic Integration of Pneumatic-Muscle-Actuator-Driven Joints into Robotic Systems via a Torque Control Interface. *Actuators* **2018**, *7*, 82. [CrossRef]

27. Ugurlu, B.; Forni, P.E.; Dallali, H.; Caldwell, D.G.; Tsagarakis, N.G. Stable Control of Force, Position, and Stiffness for a Pneumatic Muscle Actuator Joint. *Trans. Ind. Inform.* **2019**, *15*, 6270–6279. [CrossRef]
28. Hunt, A.; Szczecinski, N.; Quinn, R. Development and Training of a Neural Controller for Hind Leg Walking in a Dog Robot. *Front. Neurorobot.* **2017**, *11*, 18. [CrossRef] [PubMed]
29. Shin, T.; Kogiso, K. Sensorless angle and stiffness control of antagonistic PAM actuator using reference set. *Adv. Robot.* **2022**, *36*, 423–437. [CrossRef]
30. Winters, J.M. Hill-Based Muscle Models: A Systems Engineering Perspective. In *Multiple Muscle Systems: Biomechanics and Movement Organization*; Winters, J.M., Woo, S.L.Y., Eds.; Springer: New York, NY, USA, 1990; pp. 63–93. [CrossRef]

Disclaimer/Publisher's Note: The statements, opinions and data contained in all publications are solely those of the individual author(s) and contributor(s) and not of MDPI and/or the editor(s). MDPI and/or the editor(s) disclaim responsibility for any injury to people or property resulting from any ideas, methods, instructions or products referred to in the content.